Available online at www.sciencedirect.com

ScienceDirect

journal homepage: www.elsevier.com/locate/he

Improved H_2 detection performance of GaN sensor with Pt/Sulfide treatment of porous active layer prepared by metal electroless etching

Muhammad Shafa [a], *S. Assa Aravindh* [b], *Mohamed N. Hedhili* [c], *Saleh T. Mahmoud* [d], *Yi Pan* [a], *Tien Khee Ng* [c], *Boon S. Ooi* [c], *Adel Najar* [d,*]

[a] *State Key Laboratory for Mechanical Behavior of Materials, Xi'an Jiaotong University, Xi'an, 710049, PR China*
[b] *Nano and Molecular Systems Research Unit, University of Oulu, P.O. Box 8000, FI-90014, Oulu, Finland*
[c] *King Abdullah University of Science and Technology (KAUST), Computer, Electrical, and Mathematical Sciences and Engineering (CEMSE) Division, Thuwal, 23955-6900, Saudi Arabia*
[d] *Department of Physics, College of Science, United Arab Emirates University, Al Ain, 15551, United Arab Emirates*

HIGHLIGHTS

- High performance sulfide treated Pt/porous GaN gas sensors has been developed.
- H_2 gas sensor was working at room temperature, selective, simple, and low cost.
- Detection mechanism was investigated and supported by DFT simulations.
- A bond strengthening when Pt and S is adsorbed on porous GaN surface along with H.
- Sulfide treatment improve significantly H_2 detection at room temperature.

GRAPHICAL ABSTRACT

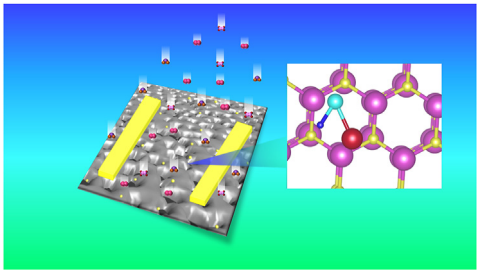

ARTICLE INFO

Article history:
Received 15 May 2020
Received in revised form
14 October 2020
Accepted 21 October 2020
Available online 16 December 2020

Keywords:
Porous GaN

ABSTRACT

High-performance chemiresistor gas sensor made of sulfide porous GaN decorated with Pt nanoparticles, which shows tunable sensor response and enhanced sensitivity. The fabricated gas sensors show detection of H_2 down to 30 ppm at 23 °C after sulfide treatment and Pt decorated porous GaN. The response time and recovery time were equal to 47 s and 113 s, respectively. Density functional theory simulations were used to support the detection mechanism based on sulfide treatment. Adsorption energy calculations showed that H adsorption energy is lowered by the simultaneous presence of S and Pt on the GaN (0001) surface. The density of states (DOS) calculations revealed possibility of bond

* *Corresponding author.*
E-mail address: adel.najar@uaeu.ac.ae (A. Najar).
https://doi.org/10.1016/j.ijhydene.2020.10.275

Surface functionalization
H_2 sensor
DFT
High sensitivity

strengthening when Pt and S is adsorbed on GaN surface along with H, arising from the hybridization of *d* and *p* orbitals of Pt and S with that of H 1s orbitals.

Introduction

The capability to identify, detect rapidly, and monitor different gases at low concentration for medical, industrial, security and even domestic applications are highly desired while working in dynamic mode. Among them, H_2, H_2S, and C_2H_4 are common pollutant gases, that pose serious risk to human health [1,2]. In this scenario, unified gas sensors that have excellent selectivity, reliability [3] high sensitivity [4], fast response, long-term stability, cost-effectiveness and low gas workable concentrations are of top priority [5–8]. Furthermore, an ample gas sensing span is requisite [9] where the fabrication of gas detectors for 10–1000 ppm of these gases is of high stakes [10]. For automotive industries and aerospace applications, gas detectors that can maneuver under highly corrosive environments and at extreme temperatures are mandatory [9,11,12]. Hence, monitoring and detecting gases rapidly and effectively has become an urgent problem to be solved. Variety of techniques have been used to build sensors to detect and monitor these pollutants, including mass spectroscopy, gas chromatography [13,14] electrochemical biosensors [15–19], optical methods [20–23] FTIR analysis [24,25], piezoelectric sensors [22–26], and chemical sensors [27].

Recently, many sensors devices based on various semiconductors materials, e.g., GaP, GaN, GaAs, AlGaAs, InGaN, InGaP, and GaN/AlGaN have been developed to produce H_2 gas sensors. I-Peing et al. fabricated a gas sensors based on Pt/GaOx/GaN gas sensors with $S_R = 1.03 \times 10^5$ under 1% H_2 and lowest detection of 1 ppm at 300 K are reported [28]. A Pd/NiO/GaN based MOS diode was reported to detect 1% H_2/air and high sensing response of 8.1×10^3 under a forward voltage of 0, 25 V at 300 K [29]. In the last few years, porous GaN becomes potentially a good candidate for gas sensor, owing to the direct band gap of this semiconductor [30] and its excellent chemical stability combined with porosity which enhances its specific surface area [31,32]. Whereas, high porosity may increase active surface area and hence the performance of the sensor will improve too. To date, etching techniques have been used to create porosity at the surface such as bottom up (dry) etching which may damage the surface of GaN [33,34]. Hence, top down (wet) etching is the best alternative as its low energy process and it is limited to the specific surface area of semiconductor, which is further divided into chemical and electrolytic etching [35–40]. Various techniques have been appraised to improve the sensitivity of the etched device, such as deposition of anti-reflection coating [41–44], gettering [45], texturing [46], dry hydrogen passivation [47], as well as coating of silicon nitride on the surface of GaN [48]. Whereas, passivation by removing metal dross provides ample space for incoming gas precipitation which may enhance the sensitivity [49]. Hence, passivation is final solution that can intensify response as well as can help the device to withstand degradation and insatiability due to oxidation. Numerous surface passivation approaches have been studied using inorganic and organic materials. Specifically, passivation through sulfide is strongly recommended for GaN, GaAs, and GaP due to formation of strong covalent bond at their surfaces [50–55]. P. Varadhan et al. addressed adverse effects of dangling bonds and chemisorbed oxide and hydroxyl ion on the surface of GaN nanowires, and demonstrated new strategy to erode these surface states by using 1,2-ethanedithiol (EDT) [56]. Indeed, passivation through 1,2-ethanedithiol (EDT) electrolyte prevents the formation of hydroxide layer at the GaN surface. Also, sensor performance can be enhanced through incorporation of noble metal elements (Pt, Pd, Au, etc.) as catalyst at the surface of the GaN [57]. These catalysts drastically improve interaction of gases with the adsorbed oxygen and hydrogen on the surface. It has been reported that Pt-coated GaN nanowires exhibit 1.7–1.9% higher response than without Pt upon exposure to H_2 [58]. Kim et al. studied room temperature GaN gas sensor based on Ga_2Pd_5 nanodots and obtained enhanced sensitivity from 34% to 63% for the detection of H_2 gas [59]. Furthermore, Lim et al. found enhanced H_2 sensitivity and response at room temperature by coating GaN nanowires with Pd nanoparticles [60]. However, combining metal nanoparticles and passivation method to enhance efficiency of the gas sensors based on porous GaN at room temperature is not yet studied.

In this work, we report a facile technique to synthesize porous GaN using metal electrochemical etching method embedded with Pt nanoparticles and passivated with EDT solution (1,2-ethanedithiol). This sulfur passivation in EDT solution was carried out for the porous surface in order to enhance the sensitivity of the sensor to detect H_2 gas. Furthermore, physical and chemical properties were investigated before the fabrication of the gas sensor. The sensitivity of chemiresistor based gas sensor was studied for H_2, H_2S and C_2H_4 gases, at various temperatures and concentrations. The selectivity, response time and recovery time were also studied. Additionally, we have also carried out first principles based density functional theory (DFT) simulations to investigate the detection mechanism based on sulfide treatment.

Materials and method

Synthesis of porous GaN, passivation and fabrication of gas sensors

The 30 μm n-type GaN film grown on sapphire substrate used in this study was purchased from Xim. Powerway Adv.

Material Co Ltd. The synthesis of porous GaN was carried out by metal electroless etching process in the solution of H_2O_2/HF/CH_3OH (2:1:2) for 30 min, as reported in our previous works [61–64]. Subsequently, EDT (99.99%, Sigma-Aldrich) solution was used to treat porous GaN samples by immersion for 5 min. Finally, Pt nanoparticles with average radius of 5 nm were deposited on porous GaN surface using an ultrahigh vacuum chamber (Mantis Deposition Ltd.). After sulfide EDT treatment and Pt nanoparticles deposition, electrical contacts of Pt/Ni with 100 nm thickness were deposited through a hard mask on the samples using a sputtering machine. The fabricated gas sensors of Pt/sulfide-porous GaN were tested under different gases (H_2S, C_2H_4, H_2) inside a chamber by varying the concentration of gas and sample temperature while nitrogen gas was used to clean the chamber after each gas flow. The gaseous flow rates were controlled by using Bronkhors mass flow meters while electrical responses of the device were monitored by computer controlled by a Keithley (KI236) source meter. The detection response was calculated as $S = Ra/Rg$, where Ra and Rg are the resistances of the gas sensor in air and under gas, respectively.

Characterization of materials

Morphological investigation of porous GaN was carried out with FEI's scanning electron microscopy (SEM) (Magellan 400 FEG) operating at 5 keV beam energy. A Bruker system (D8 Avance) was used to perform X-ray measurements on porous GaN. The photoluminescence (PL) measurements were carried out at room temperature using the Jobin Yvon LabRAM HR 800 UV system. The surface properties was investigated before and after the treatment of the surface by EDT solution. For the surface analysis, X-ray photoelectron spectroscopy (XPS) measurements was achieved with radiation source energy of $h\nu = 1486.8$ eV (Al Kα radiation source under vacuum). A 284.8 eV C 1s peaks was used to calibrate the binding energy and 'CasaXPS' software was used to analyses the data by fitting peaks with Gaussian-Lorentzian function.

Computational details

To explain the observed experimental phenomena in more detail, we modeled a two-dimensional (2D) GaN (0001) surface which was used for the DFT analysis. Initially a GaN bulk cell was optimized and the obtained a and c lattice parameters were 3.25 Å and 5.28 Å, respectively. They were used to initialize the dimensions of the 2D surface. The optimized a and c lattice parameters of the 2D surface were 6.496 Å and 30 Å respectively, such that sufficient vacuum region was included along the z orientation to make the interplay between the periodic depictions negligible. Computational studied were carried by Vienna *Ab initio* Simulation Package (VASP) with the plane wave pseudopotential code [65,66]. Spin-polarized approach was employed to describe the generalized gradient approximation (GGA) and exchange in correlation functional [67]. The pseudo potentials used were in the projected augmented wave (PAW) framework [68]. To ensure accuracy for the relaxation of atomic coordinates, force and energy tolerances of 0.001 eV/Å and 1.E-6 eV, respectively, were adopted. A kinetic energy cut-off of 400 eV was used to expand the plane waves included in the basis set. The Brillouin zone integration was carried on k-grid with 12 × 12 × 2 dimensions of Monkhorst Pack. The Hubbard U parameters, U = 6.7 eV and J = 0.7 eV for Ga [69], in the Dudarev's approach [70], were implemented in VASP because the electronic structure of GaN has a strong electronic correlations of the 3d electrons and as known that GGA approximation cannot accurately describe it.

Results and discussion

Morphology and structural characterizations

Morphological studies were carried out using SEM and the statistical information of surface porosity, mainly pore

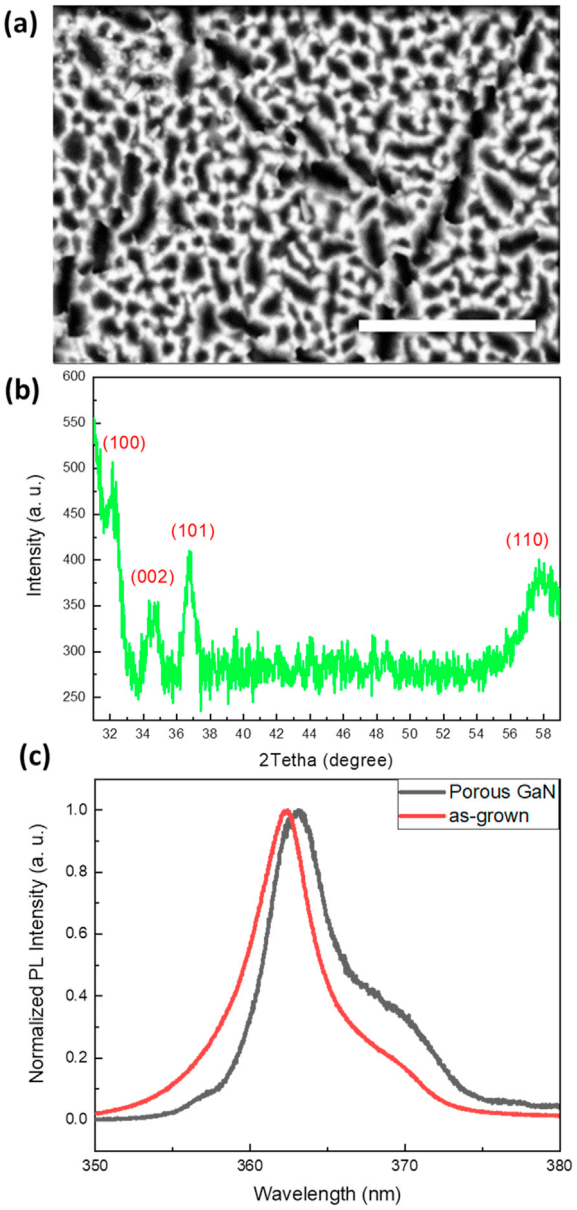

Fig. 1 – (a) SEM images of porous GaN etched for 30 min with scale bar of 1 μm. (b) XRD pattern of porous GaN. (c) PL spectra of the as grown and porous GaN.

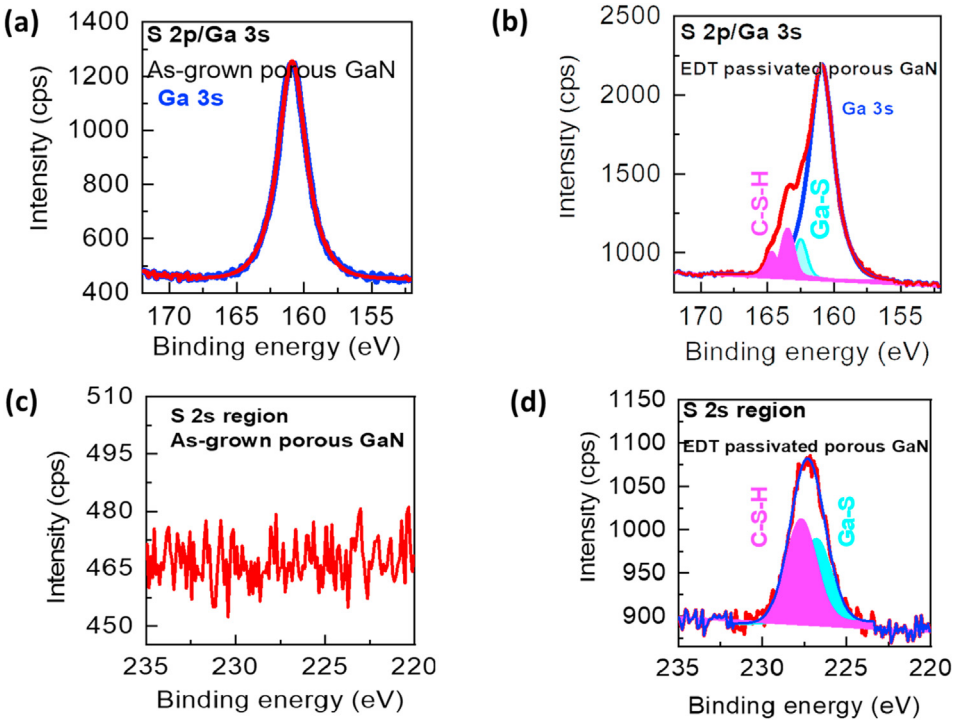

Fig. 2 – Comparison of XPS measurements of porous GaN and sulfide-treated porous GaN: (a, b) Ga 3s/S 2p region and (c, d) S 2s region of 30 min etched porous GaN.

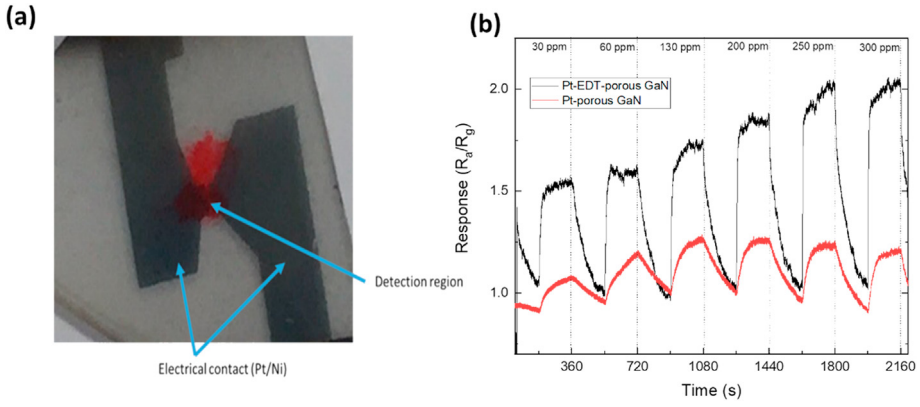

Fig. 3 – (a) Optical microscopic structure of the fabricated gas sensor with electrode and detection region. (b) Room temperature H_2 sensing response ranging from 30 ppm to 300 ppm for Pt-porous GaN untreated and treated with sulfur.

diameter distribution, was then extracted from a large number of SEM images by ImageJ software [71]. The typical image for 30 min etched sample is shown in Fig. 1a. The evaluated porosity was 58% and the mean pore diameter is around 250 nm. However, prolonged etching time may cause pores collapsed, which aggregate and form long trenches.

To confirm the crystallinity, XRD was carried out on porous GaN as shown in Fig. 1c. Based on the XRD patterns, the identification of the diffraction peaks indicates the hexagonal wurtzite GaN indexed as JCPDS card no. 898624 with a preferred orientation towards a dominant peak (002) at 34.5°, although several high index planes such (100), (002), (101) and (110) corresponding to 32.3°, 34.5°, 36.7°, and 57.8° were also observed. Among these planes the high intensity peaks correspond to (002) planes indicating the preferred orientation of the grown sample. The reflection from plane (100) correspond to high intensity with narrow peak show that surface is crystalline while (002) and (101) planes have broad peaks. Most of the peaks describe overall trend of the surface which depict that surface is closer to amorphous behavior. The lattice constants determined from diffraction peaks are a = 3.189 Å and c = 5.189 Å. The photoluminescence (PL) spectrum shown in Fig. 1c was measured on the as-grown GaN and after formation of porous GaN. The result shows that after etching, a red shift of the main PL peak from 362 nm to 363.2 nm was observed, and a small PL peak start to build up at around

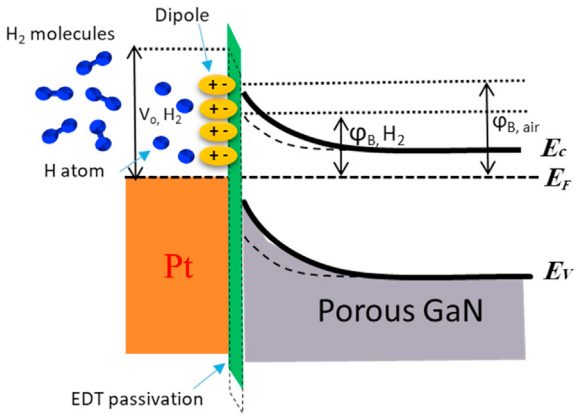

Fig. 4 – Band diagram of the Pt/passivated porous GaN under H_2 gas.

370 nm compared to the bulk is expected, due to the relaxation of compressive stress that modifies the bandgap [62,72].

The chemical composition of the pristine and EDT treated Pt/porous GaN has been investigated by XPS at ambient temperature shown in Fig. 2 in which every peak corresponds to specific binding energy value that depict its abundance. A comparative XPS studied for as grown sample and sulfur-treated porous GaN are shown in Fig. 2a–b. Due to passivation, sulfur components were introduced as shown in XPS peak at 163.4 eV corresponding to Ga 3s/S 2p while supplementary S 2p peak was accommodated using two (S $2p_{3/2}$, S $2p_{1/2}$) spin orbit coupled doublets. The sulfur contents are explained by its adsorption at the surface as Ga–S–C [73] and C–S–H [74,75] components which is attributed at 162.5 eV and 163.4 eV, respectively. After sulfur passivation of the sample, the peak shown in Fig. 2d at ~227.3 eV confirm its presence. While the peaks emerge at 226.7 eV and 227.7 eV are assigned for Ga–S [61,76] and C–S–H bonds [77], respectively, corresponding to the S 2s core level. The split is ~1 eV. The peaks positions indicate that the film consists mainly of these above-mentioned bonds. The Pt nanoparticles traces were measured with low concentration near the detection limit of the equipment (Fig. S1 of the supplementary material).

H_2 sensing properties and detection mechanism

The gas sensor devices shown in Fig. 3a were fabricated using active area composed of Pt/sulfide-porous GaN placed between two electrical contact (Pt/Ni) separated by 1 mm gap. The response of the gas sensor of porous GaN with Pt nanoparticles at room temperature before and after treatment with sulfur is depicted in Fig. 3b. The sensor exhibits a repeatable response towards H_2 gas, which varies from 40 to 59% prior to passivation at different gas concentrations such as 30–300 ppm. However, after passivation, the sensor response enhanced up to 65% at 30 ppm of H_2, such significant response for lower concentration is attributed sulfurization of the sample. Moreover, Fig. 3b shows that the response of

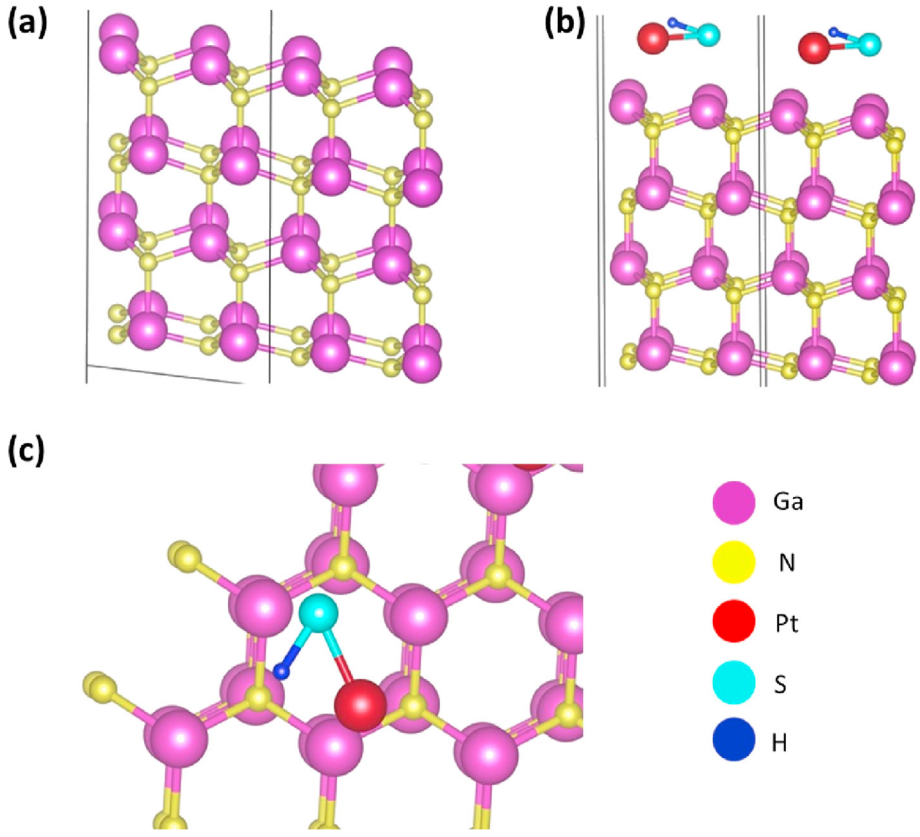

Fig. 5 – (a) and (b) show the side views of the GaN (0001) surface with and without the adsorbents. (c) shows the top view of GaN (0001) surface with Pt, H and S atoms.

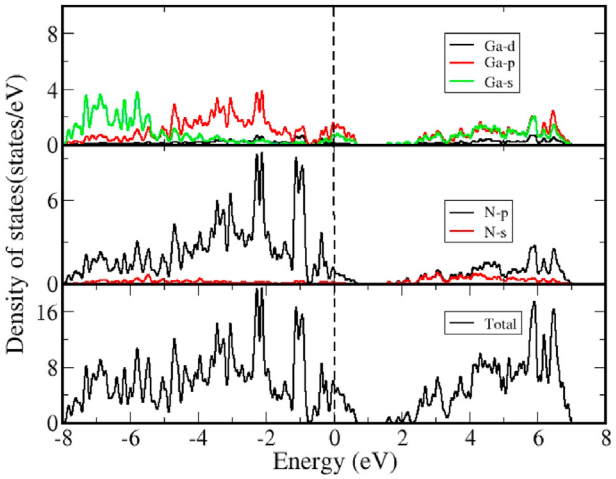

Fig. 6 – The density of states of pristine GaN (0001) surface.

untreated sample is saturated at 130 ppm of H_2 concentration. At the porous surface, this could be ascribed to the immersion of the adsorbed H_2 atoms, which may lead to surround the whole porous surface and hence hinder further adsorption and interaction of the gas with surface. The response of the sensor after sulfurization is remarkably improved by increasing the concentration of H_2 at room temperature. In our case, the detection of H_2 can be done by two methods, i) using Pt nanoparticles for porous GaN and ii) sulfide passivation of porous GaN with Pt nanoparticles. The surface of the Pt nanoparticles and the interfaces between the Pt nanoparticles and the porous GaN are crucial for the detection of H_2, since the reactions mainly occur there. When Pt NPs are exposed to H_2, the adsorption of hydrogen molecules onto the Pt surface will dissociate the molecules into H^+ (protons) due to the catalytic effect of Pt following this reaction:

$$H_2 \xrightarrow{Pt} 2H^+ + 2e^- \quad (1)$$

As the ionic radius of H^+ is much smaller than that of the Pt atoms, the H^+ can freely diffuse in the Pt lattice at room temperature and eventually captured by the N^{3+} ions at the interface of Pt nanoparticles and porous-GaN. Consequently, a dipole layer induced by H is created at the Pt/porous-GaN interface. The hydrogen sensitivity comes from the dipole layer, which significantly influences the band structure of porous-GaN [78]. However, the XPS measurements after sulfide treatment show the presence of bonding of Ga–S on the surface of porous GaN, which is favorable to detect hydrogen.

Table 1 – The adsorption energy for the GaN (0001) surface for Pt, S, H and their various combinations.

Configuration	Adsorption energy (eV)
GaN+S	−1.28
GaN+Pt	−1.20
GaN+H	0.61
GaN+Pt+H	−3.65
GaN+S+H	−2.62
GaN+Pt+S	−4.54
GaN+Pt+S+H	−5.62

For Pt/sulfide-porous GaN device will detect hydrogen based on the presence of sulfide and Pt nanoparticles on porous GaN surface.

Indeed, catalytic nature of Pt will dissociate hydrogen molecules into its constituent's i.e. hydrogen atoms and these resultant atoms diffused at the Pt/passivated porous GaN layer. At the interface, a dipole layer will be formed due to insertion of hydrogen atoms which ultimately reduce the barrier height as shown in Fig. 4. This reaction will elevate the fermi level and hence enhanced the conductivity of the passivated layer [79]. Consequently, due to this catalytic reaction, the passivated barrier $\varphi_{B,air}$ between Pt and passivated porous GaN was smoothly narrowed to $\varphi_{B,}H_2$, this reduces the resistance and hence electronic barriers between the bands. The presence of Pt nanoparticles will combine with gallium and sulfide which detect hydrogen through the hydro sulfurization that is catalyzed by metal sulfides [76]. Therefore, Pt/passivated porous GaN sensor exhibits significant response for H_2 than the Pt/porous GaN sensor because of the enhanced charge extraction which occurred due to reduction of charge recombination rate.

DFT calculations and gases detections

To understand the H_2 detection mechanism, DFT based first principal calculations have been performed. The two-dimensional (2D) GaN (0001) surface was optimized (see Fig. 5a) and the obtained intra and inter Ga–N bond lengths were 1.94 Å and 2.15 Å respectively, which is comparable to that obtained in previous studies using DFT- PBE methods [80]. Further the elements Pt, S and H were adsorbed on the GaN surface (see Fig. 5b–c) and optimization was carried out. During optimization, the layers in the bottom were fixed and the relaxation of the surface layers were allowed.

To check the characteristics of adsorption of metal atoms and hydrogen, we have calculated the adsorption energies by using Eqs. (2) and (3), respectively.

$$E_{ads}(M) = E_{GaN\_M} - E_{GaN} - \mu\, M \quad (2)$$

$$E_{ads}(H) = E_{GaN\_(M+H)} - E_{GaN\_M} - \mu H \quad (3)$$

where E_{GaN_M} and E_{GaN} in Eq. (2) represent the total energy of the GaN surface with metal atom (M) adsorbed on it and that of pristine surface respectively. The chemical potential denoted as μ is the single point energy of the respective element. Similarly, for (3), the first and second terms on the RHS signify the total energy of the GaN surface with and without H adsorbed on it. The adsorption energies are shown in Table 1.

The H adsorption energy on the pristine GaN surface is positive, but lower in magnitude. While, the negative adsorption energies for S and Pt, indicate that S and Pt can be preferably adsorbed on the GaN (0001) surface, which is supporting our experimental findings. Considering the adsorption characteristics of Pt and S, Pt is slightly more preferred. This also helps in lowering the energy while H is adsorbed in presence of Pt. The simultaneous presence of Pt and S helps in further reducing the H adsorption energy and hence will be more suitable for gas sensing.

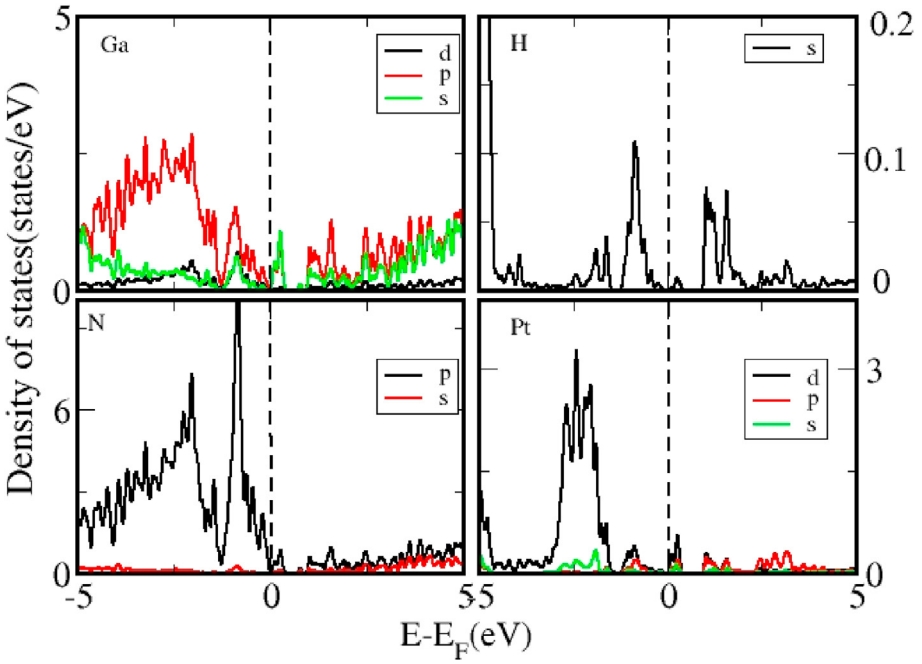

Fig. 7 – The orbital resolved DOS of GaN (0001) surface with Pt and H adsorption.

We have carried out electronic structure analysis to discern the orbital resolved contributions. Initially the density of states (DOS) of pristine GaN (0001) surface is calculated and plotted in Fig. 6.

The appearance of surface states owing to the dangling bonds can be noticed in the DOS and the occupied levels are consisting of the N-2*p* orbitals, while the *s* and *p* orbitals of Ga also contribute to a smaller extent. However, the unoccupied levels have almost equal contribution of the Ga and N atom orbitals. We also calculated the electronic structure of the GaN surface with adsorbed Pt, S and H atoms to understand the energetic preferences obtained in adsorption energy calculations. The orbital and atom resolved contributions of DOS plotted for the GaN (0001) surface with Pt and H as well as

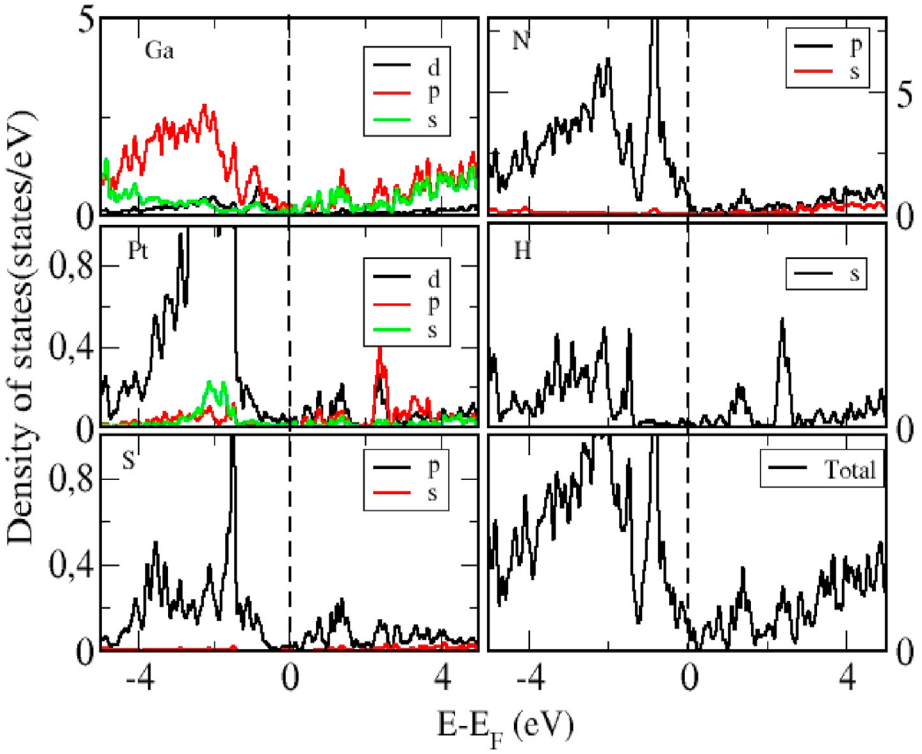

Fig. 8 – The orbital resolved DOS of GaN (0001) surface with Pt, S and H adsorption.

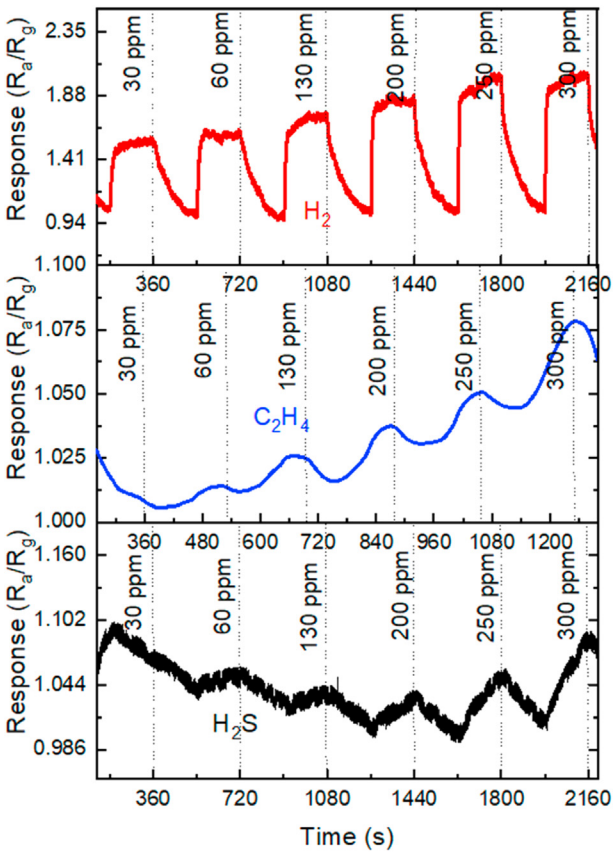

Fig. 9 – Sensor responses for H_2, C_2H_4 and H_2S gases at 23 °C.

(Pt+S) along with H are presented in Figs. 7 and 8, respectively. From Fig. 7, it can be seen that, the DOS contributed by the Pt and N orbitals at the same energy interval as that of the H 1*s* orbitals can hybridize and strengthen the bonds, which further leads to the reduction in adsorption energies for the GaN+Pt+H system. While for the GaN surface with both Pt and S coexisting with H, the *d* and *p* orbitals of Pt and Scan hybridize with the H 1*s* orbitals, rendering even stronger bonding. The band structures of pristine GaN (0001) surface and that with adsorption of H in presence of Pt and S are presented in S2 and S3 (Supporting Information), showing changes in the conducting properties and the conductivity before and after hydrogen detection.

Fig. 9 exhibits room temperature response of the sensor towards three different gasses H_2, H_2S, and C_2H_4 respectively. The figure shows that the response of the sensor increases steeply for H_2 as its concentration increases from 30 to 300 ppm. The fabricated device exhibit significant response towards H_2 at 30 ppm while second highest response corresponds to C_2H_4 due to the passivation of the sensor's active region. Though, the sensor's response for C_2H_4 gas is not uniform and independent of the gas concentration. On the other hand, the sensor's response towards H_2S gas is less than its response towards H_2 gas and it has repeatable behavior. The reason behind that could be ascribed to the filling of the porous surface with adsorbed H_2S atoms that might cease additional adsorption and interplay of the gas molecules in the active region.

Fig. 10 demonstrates the sensing response versus time of sulfur treated porous GaN with Pt nanoparticles sensors for

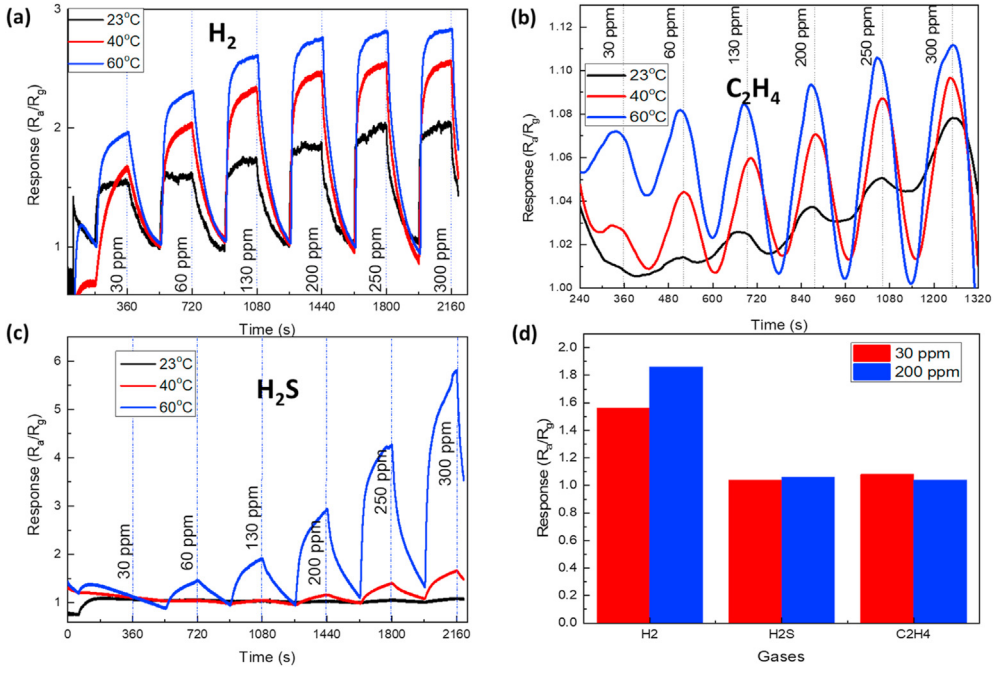

Fig. 10 – (a) Sulfide treated Pt-porous GaN sensor response for different temperatures (a) for H_2, (b) C_2H_4, and (c) H_2S. (d) Sensor responses for the H_2, H_2S, and C_2H_4 gasses at 23 °C for 30 ppm and 200 ppm.

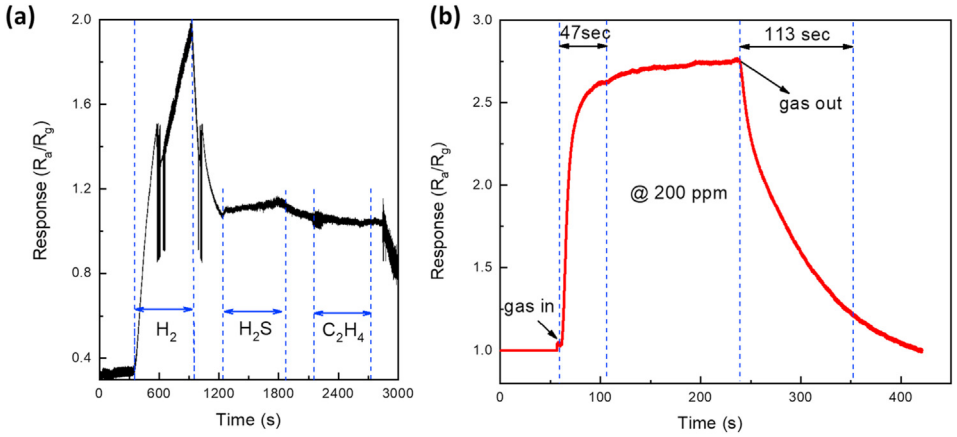

Fig. 11 – (a) Selectivity measurement of the GaN gas sensor towards H_2, H_2S and C_2H_4 for 50 ppm concentration gas for 10 min time. (b) Real and recovery times gas sensor response for 200 ppm H_2 gas at 23 °C.

different concentrations of H_2, H_2S, and C_2H_4 gases at temperatures ranging from 25 °C to 60 °C. The response of the sensor increases as the temperatures increase due to increase in surface states for interactions [81]. At lower temperatures, there is a lack of energy that support gaseous molecule to be combined with the ionic species present at porous surface and hence adsorbed. Increasing the temperature will boost the sensitivity and will reach to the saturation stage when the active region of the sensor cannot adsorb gas molecules anymore [82–84]. The responses of the sensor towards H_2 gas was higher compared to those for H_2S and C_2H_4 because the small thermal energy due to low temperature is enough to subdue the activation energy obstacle of the reaction between hydrogen and sulfur [10,85–87]. While the response of the same sensor for H_2S and C_2H_4 is lower correspond to the parameters such as availability of ionic species, activation energy barrier as well as reactive sites [10]. The response of sensor at room temperature is depicted in bar chart graph of Fig. 10d for 30 ppm and 200 ppm.

The fabricated sensor can detect broad range of gases. So, the critical parameter to analyze is the selectivity through which it can distinguish between different gases depending upon their concentrations. The selectivity test at room temperature is shown in Fig. 11a for H_2, H_2S and C_2H_4 gases at 50 ppm concentration for 10 min. The recorded sensor response at 50 ppm of H_2, H_2S, and C_2H_4 gasses are 2.00, 1.10, and 1.00, respectively. Again, the sensor's sensitivity is high towards H_2 and low for C_2H_4 gas.

There results show a sharp rise in the response during H_2 gas detection which may correspond to dangling bond recombination, while it shows a sudden rise in the response after switching the gas flow from H_2 to H_2S. Moreover, the response toward H_2S become smooth after a short interval of time and continues for 10 min. Finally, the sensor shows a weak response towards C_2H_4 gas at constant temperature and concentration. The response time is an important variable to be investigated and presented in Fig. 11b. The result reveals a rapid response time of 47 s and longer recovery time of 130 s for 200 ppm of H_2 gas. Compared to Pt/sulfide porous GaN based gas sensor, Chen et al. used GaOx passivation layer for GaN gas sensor and they achieve 13.3 s and 23.6 s for response and recovery times, respectively, however it's was measured for 10,000 ppm H2 concentration [88].

Conclusions

In summary, we fabricated H_2, H_2S, and C_2H_4 gas sensor device based on sulfide passivated porous GaN decorated with Pt nanoparticles. The fabricated device exhibit significant selectivity and sensitivity towards different gases such H_2, H_2S, and C_2H_4. Most significant performance of the gas sensor device is at room temperature, it can detect 30 ppm of H_2. In addition, Pt/sulfide porous GaN based gas sensor is also suitable for the detection of H_2S and C_2H_4 simultaneously at high temperature. The superior performance of the Pt/sulfide -GaN gas sensor is explained by DFT, for which the lowest H adsorption energy is obtained. The density of states calculations showed that there exists possibility of enhanced hybridization between the *d* and *p* orbitals of Pt and S with 1*s* orbitals of H, which may lead to the reduction in adsorption energy that subsequently leads to better H sensing properties. Moreover, the detection mechanism of H_2 gas at room temperature was investigated in detail. Selectivity response for the three gases were evaluated at 200 ppm, and a response time of 47 s have observed for H_2 gas which may correspond to disassociation and recombination time of bonding at room temperature. Our results demonstrate that environmental monitoring sensor devices can be fabricated from Pt/sulfide porous GaN, which can be promising for H_2 detection and very powerful in the future for smart city and home applications.

Declaration of competing interest

The authors declare that they have no known competing financial interests or personal relationships that could have appeared to influence the work reported in this paper.

Acknowledgements

This work was supported by Projects No. UPAR 31S443 & 31S214 from UAE University. M. Shafa and Y. Pan acknowledge the National Key R&D Program of China (2017YFA0206202), National Science Foundation of China (11704303) and China Postdoctoral Science Foundation Grant (2019M663691). S. Assa Aravindh gratefully acknowledges CSC – IT Center for Science, Finland for computational resources and Academy of Finland (#311934) for funding.

Appendix A. Supplementary data

Supplementary data to this article can be found online at https://doi.org/10.1016/j.ijhydene.2020.10.275.

REFERENCES

[1] Haouzi P, Sonobe T, Judenherc-Haouzi A. Hydrogen sulfide intoxication induced brain injury and methylene blue. Neurobiol Dis 2019. https://doi.org/10.1016/j.nbd.2019.05.013.
[2] Abdulla S, Dhakshinamoorthy J, Mohan V, Ponnuvelu DV, Kallidaikuruchi VK, Thalakkotil LM, et al. Development of low-cost hybrid multi-walled carbon nanotube-based ammonia gas-sensing strips with an integrated sensor readout system for clinical breath analyzer applications. J Breath Res 2019;13:046005. https://doi.org/10.1088/1752-7163/ab278b.
[3] Fu X, Yang P, Xiao X, Zhou D, Huang R, Zhang X, et al. Ultrafast and highly selective room-temperature formaldehyde gas sensing of Pt-decorated MoO3 nanobelts. J Alloys Compd 2019;797:666–75. https://doi.org/10.1016/j.jallcom.2019.05.145.
[4] Zhang H, Shi W, Gao N, Zhao R, Ahmed MM, Zhang T, et al. Highly sensitive and selective gas-phase ethanolamine sensor by doping sulfur into nanostructured ZnO. Sensor Actuator B Chem 2019;296:126633. https://doi.org/10.1016/j.snb.2019.126633.
[5] Yang S, Liu Y, Wu N, Zhang Y, Svoronos S, Pullammanappallil P. Low-cost, arduino-based, portable device for measurement of methane composition in biogas. Renew Energy 2019;138:224–9. https://doi.org/10.1016/j.renene.2019.01.083.
[6] Kumar M, Kumar V, Singh R. Formation of ultralong GaN nanowires up to millimeter length scale and photoconduction study in single nanowire. Scripta Mater 2017;138:75–8. https://doi.org/10.1016/j.scriptamat.2017.05.039.
[7] Song W, Wang X, Xia C, Wang R, Zhao L, Guo D, et al. Improved photoresponse of a-axis GaN microwire/p-polymer hybrid photosensor by the piezo-phototronic effect. Nano Energy 2017;33:272–9. https://doi.org/10.1016/j.nanoen.2017.01.032.
[8] Zhao D, Huang H, Chen S, Li Z, Li S, Wang M, et al. In situ growth of leakage-free direct-bridging GaN nanowires: application to gas sensors for long-term stability, low power consumption, and sub-ppb detection limit. Nano Lett 2019;19:3448–56. https://doi.org/10.1021/acs.nanolett.8b04846.
[9] Reddeppa M, Park B-G, Kim M-D, Peta KR, Chinh ND, Kim D, et al. H2, H2S gas sensing properties of rGO/GaN nanorods at room temperature: effect of UV illumination. Sensor Actuator B Chem 2018;264:353–62. https://doi.org/10.1016/j.snb.2018.03.018.
[10] Abdullah Q, Yam F, Hassan Z, Bououdina M. Hydrogen gas sensing performance of GaN nanowires-based sensor at low operating temperature. Sensor Actuator B Chem 2014;204:497–506. https://doi.org/10.1016/j.snb.2014.07.112.
[11] Pearton S, Ren F, Wang Y-L, Chu B, Chen K, Chang C, et al. Recent advances in wide bandgap semiconductor biological and gas sensors. Prog Mater Sci 2010;55:1–59. https://doi.org/10.1016/j.pmatsci.2009.08.003.
[12] Espid E, Taghipour F. UV-LED photo-activated chemical gas sensors: a review. Crit Rev Solid State Mater Sci 2017;42:416–32. https://doi.org/10.1080/10408436.2016.1226161.
[13] Lee D-Y, Huang W-C, Gu T-J, Chang G-D. Quantitative and comparative liquid chromatography-electrospray ionization-mass spectrometry analyses of hydrogen sulfide and thiol metabolites derivaitized with 2-iodoacetanilide isotopologues. J Chromatogr A 2018;1552:43–52. https://doi.org/10.1016/j.chroma.2018.04.008.
[14] Ezhilan M, Nesakumar N, Babu KJ, Srinandan C, Rayappan JBB. Freshness assessment of broccoli using electronic nose. Measurement 2019;145:735–43. https://doi.org/10.1016/j.measurement.2019.06.005.
[15] Jing A, Liang G, Shi H, Yuan Y, Zhan Q, Feng W. Three-dimensional holey-graphene architectures for highly sensitive enzymatic electrochemical determination of hydrogen peroxide. J Nanosci Nanotechnol 2019;19:7404–9. https://doi.org/10.1166/jnn.2019.16613.
[16] Colás JJ. The electro-photonic silicon biosensor. Dual-mode electro-photonic silicon biosensors. Springer; 2017. p. 59–93. https://doi.org/10.1007/978-3-319-60501-2_4.
[17] Kim J, Campbell AS, de Ávila BE-F, Wang J. Wearable biosensors for healthcare monitoring. Nat Biotechnol 2019;37:389–406. https://doi.org/10.1038/s41587-019-0045-y.
[18] Kang S-K, Murphy RK, Hwang S-W, Lee SM, Harburg DV, Krueger NA, et al. Bioresorbable silicon electronic sensors for the brain. Nature 2016;530:71–6. https://doi.org/10.1038/nature16492.
[19] Ahmad MA, Najar A, Moutaouakil AE, Nasir N, Hussein M, Raji S, et al. Label-free cancer cells detection using optical sensors. IEEE Access 2018;6:55807–14. https://doi.org/10.1109/ACCESS.2018.2872768.
[20] Eguchi K. Optical gas sensors. Gas Sensors. Springer; 1992. p. 307–28. https://doi.org/10.1007/978-94-011-2737-0_9.
[21] Jin W, Ho H, Cao Y, Ju J, Qi L. Gas detection with micro-and nano-engineered optical fibers. Opt Fiber Technol 2013;19:741–59. https://doi.org/10.1016/j.yofte.2013.08.004.
[22] Bodenhöfer K, Hierlemann A, Seemann J, Gauglitz G, Koppenhoefer B, Gpel W. Chiral discrimination using piezoelectric and optical gas sensors. Nature 1997;387:577–80. https://doi.org/10.1038/42426.
[23] Schwarz B, Reininger P, Ristanić D, Detz H, Andrews AM, Schrenk W, et al. Monolithically integrated mid-infrared lab-on-a-chip using plasmonics and quantum cascade structures. Nat Commun 2014;5:1–7. https://doi.org/10.1038/ncomms5085.
[24] Zhao R, Wang X, Liu L, Li P, Tian L. Slow pyrolysis characteristics of bamboo subfamily evaluated through kinetics and evolved gases analysis. Bioresour Technol 2019;289:121674. https://doi.org/10.1016/j.biortech.2019.121674.
[25] Nasriddinov A, Rumyantseva M, Marikutsa A, Gaskov A, Lee J-H, Kim J-H, et al. Sub-ppm formaldehyde detection by nn TiO2@ SnO2 nanocomposites. Sensors 2019;19:3182. https://doi.org/10.3390/s19143182.
[26] Khine L, Tsai JM, Heidari A, Yoon Y-J. Piezoelectric MEMS resonant gas sensor for defence applications. In: 2011

defense science research conference and expo (DSR). IEEE; 2011. p. 1–3. https://doi.org/10.1109/DSR.2011.6026862.
[27] Adib M, Eckstein R, Hernandez-Sosa G, Sommer M, Lemmer U. SnO 2 nanowire-based aerosol jet printed electronic nose as fire detector. IEEE Sensor J 2017;18:494–500. https://doi.org/10.1109/JSEN.2017.2777178.
[28] Liu IP, Chang C-H, Ke B-Y, Lin K-W. Study of a GaN Schottky diode based hydrogen sensor with a hydrogen peroxide oxidation approach and platinum catalytic metal. Int J Hydrogen Energy 2019;44:32351–61. https://doi.org/10.1016/j.ijhydene.2019.10.112.
[29] Liu IP, Chang C-H, Huang Y-M, Lin K-W. Hydrogen sensing characteristics of a Pd/Nickel oxide/GaN-based Schottky diode. Int J Hydrogen Energy 2019;44:5748–54. https://doi.org/10.1016/j.ijhydene.2019.01.056.
[30] Nord J, Nordlund K, Keinonen J, Albe K. Molecular dynamics study of defect formation in GaN cascades. Nucl Instrum Methods Phys Res Sect B Beam Interact Mater Atoms 2003;202:93–9. https://doi.org/10.1016/S0168-583X(02)01839-6.
[31] Kum H, Seong H-K, Lim W, Chun D, Kim Y-i, Park Y, et al. Wafer-scale thermodynamically stable GaN nanorods via two-step self-limiting epitaxy for optoelectronic applications. Sci Rep 2017;7:1–8. https://doi.org/10.1038/s41598-017-04426-w.
[32] Camacho-Mojica DC, López-Urías F. GaN haeckelite single-layered nanostructures: monolayer and nanotubes. Sci Rep 2015;5:17902. https://doi.org/10.1038/srep17902.
[33] Zhou S, Cao B, Liu S. Dry etching characteristics of GaN using Cl2/BCl3 inductively coupled plasmas. Appl Surf Sci 2010;257:905–10. https://doi.org/10.1016/j.apsusc.2010.07.088.
[34] Hu C-Y, Ao J-P, Okada M, Ohno Y. A study on ohmic contact to dry-etched p-GaN. IEICE Trans Electron 2008;91:1020–4. https://doi.org/10.1093/ietele/e91-c.7.1020.
[35] Hong H, Chao C, Chyi J, Tzeng Y. Reactive ion etching of GaN/InGaN using BCl3 plasma. Mater Chem Phys 2003;77:411–5. https://doi.org/10.1016/S0254-0584(02)00014-7.
[36] Youtsey C, Bulman G, Adesida I. Dopant-selective photoenhanced wet etching of GaN. J Electron Mater 1998;27:282–7. https://doi.org/10.1007/s11664-998-0400-0.
[37] Lai Y-Y, Hsu S-C, Chang H-S, Wu YS, Chen C-H, Chen L-Y, et al. The study of wet etching on GaN surface by potassium hydroxide solution. Res Chem Intermed 2017;43:3563–72. https://doi.org/10.1007/s11164-016-2430-1.
[38] Najar A, Ajlani H, Charrier J, Lorrain N, Haesaert S, Oueslati M, et al. Optical study of erbium-doped-porous silicon based planar waveguides. Phys B Condens Matter 2007;396:145–9. https://doi.org/10.1016/j.physb.2007.03.034.
[39] Najar A, Charrier J, Ajlani H, Lorrain N, Elhouichet H, Oueslati M, et al. Optical properties of erbium-doped porous silicon waveguides. J Lumin 2006;121:245–8. https://doi.org/10.1016/j.jlumin.2006.08.072.
[40] Najar A, Charrier J, Lorrain N, Haji L, Oueslati M. Optical gain measurements in porous silicon planar waveguides codoped by erbium and ytterbium ions at 1.53μm. Appl Phys Lett 2007;91:121120. https://doi.org/10.1063/1.2789185.
[41] Kang D-W, Kwon J-Y, Shim J, Lee H-M, Han M-K. Highly conductive GaN anti-reflection layer at transparent conducting oxide/Si interface for silicon thin film solar cells. Sol Energy Mater Sol Cells 2012;105:317–21. https://doi.org/10.1016/j.solmat.2012.06.041.
[42] Hsu C-H, Chan Y-C, Chen W-C, Chang C-H, Liou J-K, Cheng S-Y, et al. Study of GaN-based LEDs with hybrid SiO 2 microsphere/nanosphere antireflection coating as a passivation layer by a rapid convection deposition. IEEE Trans Electron Dev 2017;64:1134–9. https://doi.org/10.1109/TED.2017.2657659.
[43] Najar A, Omi H, Tawara T. Effect of structure and composition on optical properties of Er-Sc silicates prepared from multi-nanolayer films. Opt Express 2015;23:7021–30. https://doi.org/10.1364/OE.23.007021.
[44] Najar A, Omi H, Tawara T. Scandium effect on the luminescence of Er-Sc silicates prepared from multi-nanolayer films. Nanoscale Res Lett 2014;9:356. https://doi.org/10.1186/1556-276X-9-356.
[45] Majid A, Ali A, Zhu J, Wang Y, Yang H. An evidence of defect gettering in GaN. Phys B Condens Matter 2008;403:2495–9. https://doi.org/10.1016/j.physb.2008.01.012.
[46] Kim D-w, Yu S-J, Seo J-O, Kim H-T, Seo J-W. Light extraction improvement of 400 nm wavelength GaN-based light-emitting diode by textured structures. J Korea Acad Industr coop Soc 2009;10:1514–9. https://doi.org/10.5762/KAIS.2009.10.7.1514.
[47] Götz W, Johnson N, Walker J, Bour D, Amano H, Akasaki I. Hydrogen passivation of Mg acceptors in GaN grown by metalorganic chemical vapor deposition. Appl Phys Lett 1995;67:2666–8. https://doi.org/10.1063/1.114330.
[48] Gatabi IR, Johnson DW, Woo JH, Anderson JW, Coan MR, Piner EL, et al. PECVD silicon nitride passivation of AlGaN/GaN heterostructures. IEEE Trans Electron Dev 2013;60:1082–7. https://doi.org/10.1109/TED.2013.2242075.
[49] Liu S-C, Chen B-Y, Lin Y-C, Hsieh T-E, Wang H-C, Chang EY. GaN MIS-HEMTs with nitrogen passivation for power device applications. IEEE Electron Device Lett 2014;35:1001–3. https://doi.org/10.1109/LED.2014.2345130.
[50] Zhao C, Ng TK, Prabaswara A, Conroy M, Jahangir S, Frost T, et al. An enhanced surface passivation effect in InGaN/GaN disk-in-nanowire light emitting diodes for mitigating Shockley–Read–Hall recombination. Nanoscale 2015;7:16658–65. https://doi.org/10.1039/C5NR03448E.
[51] Khan JI, Adhikari A, Sun J, Priante D, Bose R, Shaheen BS, et al. Enhanced optoelectronic performance of a passivated nanowire-based device: Key information from real-space imaging using 4D electron microscopy. Small 2016;12:2313–20. https://doi.org/10.1002/smll.201503651.
[52] Chen W, Li X, Duan L, Xie X, Cui Y. Photoluminescence enhancement of (NH4) 2Sx passivated InP surface by rapid thermal annealing. Appl Surf Sci 1996;100:592–5. https://doi.org/10.1016/0169-4332(96)00345-5.
[53] Sun M, Joyce HJ, Gao Q, Tan H, Jagadish C, Ning C-Z. Removal of surface states and recovery of band-edge emission in InAs nanowires through surface passivation. Nano Lett 2012;12:3378–84. https://doi.org/10.1021/nl300015w.
[54] Tajik N, Haapamaki C, LaPierre R. Photoluminescence model of sulfur passivated p-InP nanowires. Nanotechnology 2012;23:315703. https://doi.org/10.1088/0957-4484/23/31/315703.
[55] Lee C-S, Lin Y-J, Lee C-T. Investigation of oxidation mechanism for ohmic formation in Ni/Au contacts to p-type GaN layers. Appl Phys Lett 2001;79:3815–7. https://doi.org/10.1063/1.1425065.
[56] Varadhan P, Fu H-C, Priante D, Retamal JRD, Zhao C, Ebaid M, et al. Surface passivation of GaN nanowires for enhanced photoelectrochemical water-splitting. Nano Lett 2017;17:1520–8. https://doi.org/10.1021/acs.nanolett.6b04559.
[57] Mirzaei A, Yousefi HR, Falsafi F, Bonyani M, Lee J-H, Kim J-H, et al. An overview on how Pd on resistive-based nanomaterial gas sensors can enhance response toward hydrogen gas. Int J Hydrogen Energy 2019. https://doi.org/10.1016/j.ijhydene.2019.05.180.
[58] Wright J, Lim W, Gila B, Pearton S, Johnson JL, Ural A, et al. Hydrogen sensing with Pt-functionalized GaN nanowires. Sensor Actuator B Chem 2009;140:196–9. https://doi.org/10.1016/j.snb.2009.04.009.

[59] Kim SS, Park JY, Choi S-W, Kim HS, Na HG, Yang JC, et al. Room temperature sensing properties of networked GaN nanowire sensors to hydrogen enhanced by the Ga2Pd5 nanodot functionalization. Int J Hydrogen Energy 2011;36:2313–9. https://doi.org/10.1016/j.ijhydene.2010.11.050.
[60] Lim W, Wright J, Gila B, Johnson JL, Ural A, Anderson T, et al. Room temperature hydrogen detection using Pd-coated GaN nanowires. Appl Phys Lett 2008;93:072109. https://doi.org/10.1063/1.2975173.
[61] Najar A, Gerland M, Jouiad M. Porosity-induced relaxation of strains in GaN layers studied by means of micro-indentation and optical spectroscopy. J Appl Phys 2012;111:093513. https://doi.org/10.1063/1.4710994.
[62] Najar A, Shafa M, Anjum D. Synthesis, optical properties and residual strain effect of GaN nanowires generated via metal-assisted photochemical electroless etching. RSC Adv 2017;7:21697–702. https://doi.org/10.1039/C7RA02348K.
[63] Najar A, Jouiad M. Synthesis of InGaN nanowires via metal-assisted photochemical electroless etching for solar cell application. Sol Energy Mater Sol Cell 2018;180:243–6. https://doi.org/10.1016/j.solmat.2017.06.008.
[64] Slimane AB, Najar A, Elafandy R, San-Román-Alerigi DP, Anjum D, Ng TK, et al. On the phenomenon of large photoluminescence red shift in GaN nanoparticles. Nanoscale Res Lett 2013;8:342. https://doi.org/10.1186/1556-276X-8-342.
[65] Kresse G, Furthmüller J. Efficient iterative schemes for ab initio total-energy calculations using a plane-wave basis set. Phys Rev B 1996;54:11169. https://doi.org/10.1103/PhysRevB.54.11169.
[66] Kresse G, Hafner J. Ab initio molecular dynamics for liquid metals. Phys Rev B 1993;47:558. https://doi.org/10.1103/physrevb.47.558.
[67] Blöchl PE. Projector augmented-wave method. Phys Rev B 1994;50:17953. https://doi.org/10.1103/PhysRevB.50.17953.
[68] Perdew JP, Wang Y. Accurate and simple analytic representation of the electron-gas correlation energy. Phys Rev B 1992;45:13244. https://doi.org/10.1103/PhysRevB.45.13244.
[69] Aravindh SA, Roqan IS. Defect-impurity complex induced long-range ferromagnetism in GaN nanowires. Mater Res Express 2015;2:126104. https://doi.org/10.1088/2053-1591/2/12/126104.
[70] Dudarev S, Botton G, Savrasov S, Humphreys C, Sutton A. Electron-energy-loss spectra and the structural stability of nickel oxide: an LSDA+ U study. Phys Rev B 1998;57:1505. https://doi.org/10.1103/PhysRevB.57.1505.
[71] Goldstein JI, Newbury DE, Michael JR, Ritchie NW, Scott JHJ, Joy DC. ImageJ and Fiji. Scanning electron microscopy and X-ray microanalysis. Springer; 2018. p. 187–93. https://doi.org/10.1007/978-1-4939-6676-9.
[72] Assa Aravindh S, Xin B, Mitra S, Roqan IS, Najar A. GaN and InGaN nanowires prepared by metal-assisted electroless etching: experimental and theoretical studies. Results Phys 2020;19:103428. https://doi.org/10.1016/j.rinp.2020.103428.
[73] Castner DG, Hinds K, Grainger DW. X-ray photoelectron spectroscopy sulfur 2p study of organic thiol and disulfide binding interactions with gold surfaces. Langmuir 1996;12:5083–6. https://doi.org/10.1021/la960465w.
[74] Joseph Y, Besnard I, Rosenberger M, Guse B, Nothofer H-G, Wessels JM, et al. Self-assembled gold nanoparticle/alkanedithiol films: preparation, electron microscopy, XPS-analysis, charge transport, and vapor-sensing properties. J Phys Chem B 2003;107:7406–13. https://doi.org/10.1021/jp030439o.
[75] Madaan N, Romriell N, Tuscano J, Schlaad H, Linford MR. Introduction of thiol moieties, including their thiol–ene reactions and air oxidation, onto polyelectrolyte multilayer substrates. J Colloid Interface Sci 2015;459:199–205. https://doi.org/10.1016/j.jcis.2015.08.017.
[76] Shafa M, Priante D, ElAfandy RT, Hedhili MN, Mahmoud ST, Ng TK, et al. Twofold porosity and surface functionalization effect on Pt–porous GaN for high-performance H2-gas sensors at room temperature. ACS Omega 2019;4:1678–84. https://doi.org/10.1021/acsomega.8b02730.
[77] Guo W, Liu T, Zhang H, Sun R, Chen Y, Zeng W, et al. Gas-sensing performance enhancement in ZnO nanostructures by hierarchical morphology. Sensor Actuator B Chem 2012;166:492–9. https://doi.org/10.1016/j.snb.2012.02.093.
[78] Baik KH, Kim J, Jang S. Highly sensitive nonpolar a-plane GaN based hydrogen diode sensor with textured active area using photo-chemical etching. Sensor Actuator B Chem 2017;238:462–7. https://doi.org/10.1016/j.snb.2016.07.091.
[79] Trinchi A, Kaciulis S, Pandolfi L, Ghantasala M, Li Y, Wlodarski W, et al. Characterization of Ga2O3 based MRISiC hydrogen gas sensors. Sensor Actuator B Chem 2004;103:129–35. https://doi.org/10.1016/j.snb.2004.04.112.
[80] Landmann M, Rauls E, Schmidt W, Neumann M, Speiser E, Esser N. GaN m-plane: atomic structure, surface bands, and optical response. Phys Rev B 2015;91:035302. https://doi.org/10.1103/PhysRevB.91.035302.
[81] Xie L, Sun L, Dong B, Fatima Q, Wang Z, Yao Z, et al. Sol-gel synthesis of TiO2 with p-type response to hydrogen gas at elevated temperature. Frontiers in Materials 2019;6:184. https://doi.org/10.3389/fmats.2019.00096.
[82] Zhang S, Chen H-S, Matras-Postolek K, Yang P. ZnO nanoflowers with single crystal structure towards enhanced gas sensing and photocatalysis. Phys Chem Chem Phys 2015;17:30300–6. https://doi.org/10.1039/C5CP04860E.
[83] Li X, Zhou X, Guo H, Wang C, Liu J, Sun P, et al. Design of Au@ZnO yolk–shell nanospheres with enhanced gas sensing properties. ACS Appl Mater Interfaces 2014;6:18661–7. https://doi.org/10.1021/am5057322.
[84] Sun P, Zhou X, Wang C, Shimanoe K, Lu G, Yamazoe N. Hollow SnO 2/α-Fe 2 O 3 spheres with a double-shell structure for gas sensors. J Mater Chem 2014;2:1302–8. https://doi.org/10.1039/C3TA13707D.
[85] Yan J-T, Lee C-T. Improved detection sensitivity of Pt/β-Ga2O3/GaN hydrogen sensor diode. Sensor Actuator B Chem 2009;143:192–7. https://doi.org/10.1016/j.snb.2009.08.040.
[86] Abdullah Q, Yam F, Hassan J, Chin C, Hassan Z, Bououdina M. High performance room temperature GaN-nanowires hydrogen gas sensor fabricated by chemical vapor deposition (CVD) technique. Int J Hydrogen Energy 2013;38:14085–101. https://doi.org/10.1016/j.ijhydene.2013.08.014.
[87] Lee J-H. Gas sensors using hierarchical and hollow oxide nanostructures: overview. Sensor Actuator B Chem 2009;140:319–36. https://doi.org/10.1016/j.snb.2009.04.026.
[88] Chen C-C, Chen H-I, Liu IP, Liu H-Y, Chou P-C, Liou J-K, et al. Enhancement of hydrogen sensing performance of a GaN-based Schottky diode with a hydrogen peroxide surface treatment. Sensor Actuator B Chem 2015;211:303–9. https://doi.org/10.1016/j.snb.2015.01.099.